REDOR Dephasing by Multiple Spins in the Presence of Molecular Motion

Jon M. Goetz and Jacob Schaefer

Department of Chemistry, Washington University, St. Louis, Missouri 63130

Closed-form, numerical algorithms are presented for calculating REDOR dephasing for three general cases: (i) collections of isolated I–S spin pairs; (ii) many S spins coupled to an I spin; and (iii) an I–S spin pair in relative motion. For the case when more than one S spin is dipolar coupled to an I spin, the calculation assumes that the S–S homonuclear interaction does not affect REDOR dephasing. Full numerical simulations show that this assumption is true if the S-spin lineshapes are inhomogeneously broadened, the S-spin chemical shifts are far from rotational resonance, and a version of REDOR is used which minimizes the number of S-spin π pulses. For the rapidly rotating $-CF_3$ group of poly(trifluoroethyl methacrylate), the formalisms of (ii) and (iii) are combined to calculate the dephasing. The experimentally measured dephasing matches theory when the wiggling motion of the $-OCH_2CF_3$ moiety of the polymer is taken into account. © 1997 Academic Press

INTRODUCTION

Magic-angle spinning is a well-established method for obtaining high-resolution spectra in solids. If the rotor axis is aligned at the magic angle, all second-rank interactions are averaged to zero over a rotor period (*1*). For the chemical-shift interaction, the removal of second-rank or anisotropic terms is generally desirable because this results in high-resolution spectra. Schemes for recovering the chemical information contained in the shift anisotropy from residual sidebands are available (*2*).

Distance-dependent dipole–dipole couplings are also second-rank interactions averaged to zero over a rotor period. Rotational-echo double resonance (REDOR) experiments have been designed to reintroduce these weak, heteronuclear dipolar interactions during magic-angle spinning experiments (*3, 4*). The REDOR experiment uses rotor-synchronized π pulses to defeat magic-angle spinning motional averaging of heteronuclear dipole–dipole interactions. The result is a loss of rotational-echo amplitude. The signal intensity with (S) and without (S_0) the dephasing π pulses is measured in an alternate-block experiment. For a collection of static, equidistant, isolated heteronuclear pairs, the normalized loss of the rotational-echo signal (S/S_0) is a simple, analytical

function of the number of rotor cycles, the rotor period, and the strength of the heteronuclear dipole–dipole interaction (*5, 6*). For isolated pairs, the strength of the interaction is proportional to the inverse cube of the internuclear distance. This technique has been successfully applied to give accurate measures of distances between isolated spin pairs in a number of structural studies (*7, 8*).

This paper describes how to calculate REDOR dephasing when the assumption of equidistant, isolated, static heteronuclear pairs is relaxed. Algorithms are presented for calculating REDOR dephasing when (i) the isolated pairs have a distribution of internuclear distances; (ii) the observed spin is coupled to more than one other spin; and (iii) the spins are in relative motion. Techniques (ii) and (iii) are combined to calculate ^{13}C REDOR dephasing by ^{19}F in a trifluoromethyl group undergoing rapid rotation about its C_3 axis. Dephasing observed for the $-CF_3$ carbon in natural-abundance poly(trifluoroethyl methacrylate) is in agreement with theory.

THEORY

Isolated I–S Spin Pair

The dipolar coupling between an I–S heteronuclear spin pair (Fig. 1) is a function of time for a sample spinning at the magic angle. Assuming that the I–S internuclear vector is fixed in the rotor at a polar angle β and an azimuthal angle α, the dipolar coupling in hertz is $\nu_D(\alpha, \beta; t)$ (*3*),

$$\nu_D(\alpha, \beta; t) = \frac{\nu_D}{2} [\sin^2\beta \cos 2(\alpha + 2\pi\nu_D t) - \sqrt{2} \sin 2\beta \cos(\alpha + 2\pi\nu_D t)], \quad [1]$$

where

$$\nu_D = \frac{h\gamma_I\gamma_S}{4\pi^2 r_{I-S}^3} \quad [2]$$

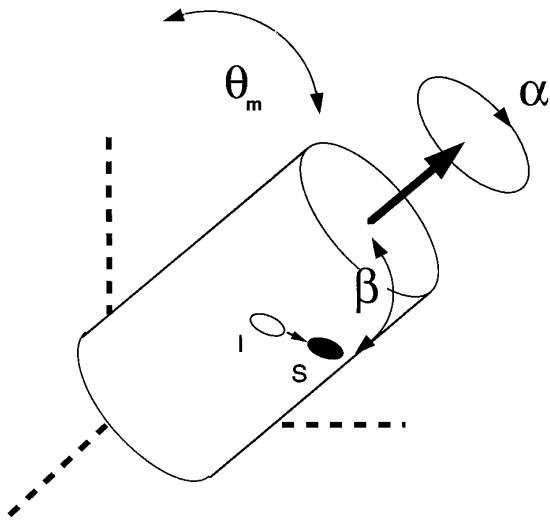and ν_R is the rotor speed in hertz; γ_I and γ_S are the I and S

FIG. 1. Rose-convention Euler angles describing the orientation of an *I–S* spin pair in a sample which rotates at the magic angle. The rotor axis is aligned at the magic angle, θ_m. The polar and azimuthal angles, β and α, respectively, describe the orientation of the *I–S* internuclear vector which is fixed in the rotor frame.

gyromagnetic ratios, respectively; and r_{I-S} is the internuclear separation (*3*).

During a single rotor cycle, *I*-observe, *S*-dephase REDOR experiment, an inverting π pulse is applied at the *S*-spin resonance frequency. For maximum dephasing, the π pulse is placed in the middle of the rotor cycle (*5*). The *I*-spin magnetization is measured with (*S*) and without (*S_0*) application of the dephasing π pulse. The time evolution of the spin density matrix $\rho(t)$ is

$$\rho(t) = e^{-i\Theta(t,0)I_Z S_Z}\rho(0)e^{+i\Theta(t,0)I_Z S_Z}, \qquad [3]$$

where I_Z and S_Z are the z components of the spin angular-momentum operators for *I* and *S* spins, respectively, and

$$\Theta(t_2, t_1) = 2\pi \int_{t_1}^{t_2} \nu_D(\alpha, \beta; t)dt. \qquad [4]$$

If the *I*-spin magnetization is placed along the x axis with a $\pi/2$ pulse at $t = 0$, then $\rho(0) = M_0 I_x$. After one rotor cycle of REDOR with a dephasing *S*-spin π pulse in the middle of the rotor period, the density matrix becomes $\rho(T_R)$, where

$$\rho(T_R) = M_0 I_x \cos\left[\frac{\nu_D}{\nu_R} 2\sqrt{2} \sin 2\beta \sin \alpha\right]$$

$$+ 2M_0 I_y S_z \sin\left[\frac{\nu_D}{\nu_R} 2\sqrt{2} \sin 2\beta \sin \alpha\right]. \quad [5]$$

The NMR signal is obtained by evaluating the trace of $\rho(t)$

with $I_+ = I_x + iI_y$. The ratio of the observable *I*-spin signal with and without the *S*-spin π pulse for an *I–S* spin pair oriented along (α, β) in the rotor frame is

$$\frac{S(\alpha, \beta)}{S_0} = \cos\left[\frac{\nu_D}{\nu_R} 2\sqrt{2} \sin 2\beta \sin \alpha\right]. \qquad [6]$$

If π pulses are placed every half rotor period, the REDOR pulse sequence is cyclic. Therefore, after N_C rotor cycles of REDOR, Eq. [6] has the same form except ν_D is replaced by $N_C \nu_D$ (*3*).

If the sample is amorphous or powdered, an isotropic distribution of *I–S* spin pair orientations is assumed. The observed REDOR dephasing (S/S_0) is calculated by performing the standard powder average or
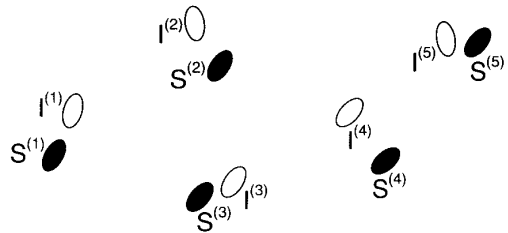
$$\frac{S}{S_0} = \frac{1}{4\pi} \int_{\alpha=0}^{2\pi} \int_{\beta=0}^{\pi} \cos\left[\frac{N_C\nu_D}{\nu_R} 2\sqrt{2} \sin 2\beta \sin \alpha\right]$$

$$\times d\alpha \sin \beta d\beta. \qquad [7]$$
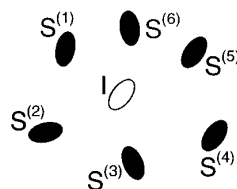
Collections of Isolated I–S Spin Pairs

In some heterogeneous systems, the assumption that all spin pairs are equidistant needs to be relaxed. For the situation pictured in Fig. 2a, the pairs are isolated but not equidistant. The density matrix after a $\pi/2$ inspection pulse is

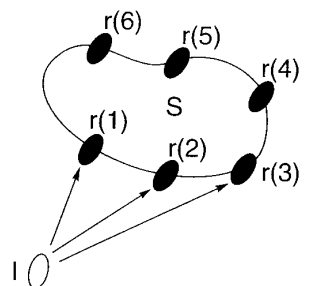$$\rho(0) = I_x^{(1)} + I_x^{(2)} + \cdots, \qquad [8]$$

FIG. 2. Three possibilities for *I*-spin REDOR with *S*-spin dephasing.

where $I_x^{(i)}$ is the x component of the spin angular-momentum operator for the ith I spin. The time evolution of the density matrix is

$$\rho(t) = e^{[-i\Theta(t,0)I_z^{(1)}S_z^{(1)} - i\Theta(t,0)I_z^{(2)}S_z^{(2)} - \cdots]}$$
$$\times \rho(0)e^{[i\Theta(t,0)I_z^{(1)}S_z^{(1)} + i\Theta(t,0)I_z^{(2)}S_z^{(2)} + \cdots]}, \quad [9]$$

where $I_z^{(i)}$ and $S_z^{(i)}$ are the z components of the spin angular-momentum operator for the ith I and S spins, respectively. Because the operators commute, $[I^{(i)}, I^{(j)}] = 0$ and $[S^{(i)}, S^{(j)}] = 0$, the density matrix reduces to a sum of terms

$$\rho(t) = e^{[-i\Theta(t,0)I_z^{(1)}S_z^{(1)}]} I_x^{(1)} e^{[i\Theta(t,0)I_z^{(1)}S_z^{(1)}]}$$
$$+ e^{[-i\Theta(t,0)I_z^{(2)}S_z^{(2)}]} I_x^{(2)} e^{[i\Theta(t,0)I_z^{(2)}S_z^{(2)}]} + \cdots. \quad [10]$$

Each of the terms in the sum of Eq. [10] represents the REDOR dephasing for an individual $I–S$ spin pair. The observed dephasing is therefore a sum of REDOR curves:

$$\frac{S}{S_0} = \frac{1}{4\pi} \int_{\alpha=0}^{2\pi} \int_{\beta=0}^{\pi} \cos\left[\frac{\nu_D^{(1)}}{\nu_R} 2\sqrt{2} \sin 2\beta \sin \alpha\right]$$

$$\times d\alpha \sin \beta d\beta + \frac{1}{4\pi} \int_{\alpha=0}^{2\pi} \int_{\beta=0}^{\pi}$$

$$\times \cos\left[\frac{\nu_D^{(2)}}{\nu_R} 2\sqrt{2} \sin 2\beta \sin \alpha\right]$$

$$\times d\alpha \sin \beta d\beta + \cdots. \quad [11]$$

In this case, the experimentally measured dephasing can be fit using a model distribution of internuclear distances and the resulting sum of REDOR dephasing curves (9, 10), or the distribution can be measured directly by performing a REDOR transform of the observed dephasing (6). An advantage of the REDOR transform is that it gives model-independent distributions; a disadvantage is that it requires highly accurate S/S_0 time-domain data when S is small, a technically demanding requirement.

Many S Spins Coupled to an I Spin

If more than one S spin is coupled to the observed I spin, as depicted in Fig. 2b, the time evolution of the density matrix under *only* the $I–S$ heteronuclear dipolar interaction after a $\pi/2$ inspection pulse is

$$\rho(t) = e^{[-i\Theta(t,0)I_zS_z^{(1)} - i\Theta(t,0)I_zS_z^{(2)} - \cdots]}$$
$$\times I_x e^{[i\Theta(t,0)I_zS_z^{(1)} + i\Theta(t,0)I_zS_z^{(2)} + \cdots]}. \quad [12]$$

In other words, Eq. [12] is valid when the S-spin homonuclear interaction can be neglected, that is, when

$$\Theta(t, 0) \times \sum_{i,j} \left[S_z^{(i)}S_z^{(j)} - \frac{1}{4}(S_+^{(i)}S_-^{(j)} + S_-^{(i)}S_+^{(j)}) \right] = 0.$$
$$[13]$$

Because the exponential terms in Eq. [12] commute,

$$\rho(t) = \cdots e^{[-i\Theta(t,0)I_zS_z^{(2)}]} e^{[-i\Theta(t,0)I_zS_z^{(1)}]}$$
$$\times I_x e^{[i\Theta(t,0)I_zS_z^{(1)}]} e^{[i\Theta(t,0)I_zS_z^{(2)}]} \cdots. \quad [14]$$

Evaluating the propagator closest to the I_x operator first gives

$$\rho(t) = \cdots e^{[-i\Theta(t,0)I_zS_z^{(2)}]} I_x$$
$$\times \cos\left[\frac{\nu_D^{(1)}}{\nu_R} 2\sqrt{2} \sin 2\beta^{(1)}\sin \alpha^{(1)}\right]$$
$$\times e^{[i\Theta(t,0)I_zS_z^{(2)}]} \cdots. \quad [15]$$

Each coupled spin introduces another cosine term to the expression. The total dephasing for the system is therefore a *product* of cosine terms (11, 12):

$$\frac{S}{S_0} = \frac{1}{8\pi^2} \int d\Omega \cos\left[\frac{N_C\nu_D^{(1)}}{\nu_R} 2\sqrt{2} \sin 2\beta^{(1)}\sin \alpha^{(1)}\right]$$

$$\times \cos\left[\frac{N_C\nu_D^{(2)}}{\nu_R} 2\sqrt{2} \sin 2\beta^{(2)}\sin \alpha^{(2)}\right] \times \cdots.$$
$$[16]$$

To perform the powder average, the integral must include all possible orientations of the collection of S spins. As for any solid body, three Euler angles (ϕ, θ, ψ) (13) are required to specify this orientation. The $(\sin 2\beta^{(i)}\sin \alpha^{(i)})$ terms in Eq. [16] must therefore be expressed as a function of these three Euler angles.

To derive this expression, we define the unit vector from the I spin to the $S^{(i)}$ spin as $\hat{n}(i) = \mathbf{r}_{IS}^{(i)}/|\mathbf{r}_{IS}^{(i)}| = (\hat{x}(i), \hat{y}(i), \hat{z}(i))$. Rotating this unit vector by (ϕ, θ, ψ) gives a new unit vector, $\hat{n}'(i)$, defined by

$$\hat{n}'(i) = \mathbf{A}(\phi, \theta, \psi)\cdot \hat{n}(i), \quad [17]$$

where $\mathbf{A}(\phi, \theta, \psi)$ is the 3×3 Eulerian rotation matrix (13). After this rotation, projections of the rotated unit vector are expressed in terms of α and β as

$$\hat{n}'(i)\cdot \hat{x} = \sin \beta^{(i)}\cos \alpha^{(i)}$$
$$\hat{n}'(i)\cdot \hat{y} = \sin \beta^{(i)}\sin \alpha^{(i)}$$
$$\hat{n}'(i)\cdot \hat{z} = \cos \beta^{(i)}. \quad [18]$$

Assuming an Euler rotation in the Rose convention (13),

$$\hat{n}'(i) \cdot \hat{z} = [\sin \theta \cos \phi] \hat{x}(i)$$
$$+ [\sin \theta \sin \phi] \hat{y}(i) + [\cos \theta] \hat{z}(i) \quad [19]$$

and

$$\hat{n}'(i) \cdot \hat{y} = [-\cos \psi \sin \phi - \cos \theta \cos \phi \sin \psi] \hat{x}(i)$$
$$+ [\cos \psi \cos \phi - \cos \theta \sin \phi \sin \psi] \hat{y}(i)$$
$$+ [\sin \psi \sin \theta] \hat{z}(i). \quad [20]$$

It is now possible to evaluate the argument of the cosine term in Eq. [16] using

$$\sin 2\beta^{(i)} \sin \alpha^{(i)} = 2 \cos \beta^{(i)} \sin \beta^{(i)} \sin \alpha^{(i)}$$
$$= 2[\hat{n}'(i) \cdot \hat{y}][\hat{n}'(i) \cdot \hat{z}]. \quad [21]$$

The closed-form expression for the powder integral in the presence of more than one S spin is a function of the number of rotor cycles (N_C), the spinning speed in hertz (ν_R), the strength of the I–S dipolar coupling for the ith S spin ($\nu_D^{(i)} = h\gamma_I\gamma_S/[4\pi|\mathbf{r}_{IS}^{(i)}|^3]$), the internuclear unit vector ($\hat{n}(i)$), and the three Euler angles (ϕ, θ, ψ). The expression is

$$\frac{S}{S_0} = \frac{1}{8\pi^2} \int_{\psi=0}^{2\pi} \int_{\theta=0}^{\pi} \int_{\phi=0}^{2\pi} \prod_i$$
$$\times \cos\left[\frac{N_C \nu_D^{(i)}}{\nu_R} 4\sqrt{2}[\hat{n}'(i) \cdot \hat{y}][\hat{n}'(i) \cdot \hat{z}]\right]$$
$$\times d\phi \sin \theta d\theta d\psi. \quad [22]$$

Motional Averaging

Relative motion of a heteronuclear spin pair, as shown in Fig. 2c, has an effect on REDOR dephasing if the motion occurs on time scales which are shorter than the reciprocal of the dipole–dipole interaction. In this case, $\Theta(t, 0)$ is time averaged and the density matrix is

$$\rho(t) = e^{[-i\overline{\Theta(t,0)}I_Z S_Z]} I_X e^{[i\overline{\Theta(t,0)}I_Z S_Z]}, \quad [23]$$

where $\overline{\Theta(t, 0)}$ is the time-averaged interaction. This term can be calculated if the relative trajectory of the two spins is known. The position of the S spin relative to the fixed I spin for any time, t_i, is

$$\mathbf{r}(i) = [x(t_i), y(t_i), z(t_i)]. \quad [24]$$

As the S spin moves through its trajectory in N steps of duration Δt, the time-averaged interaction is

$$\overline{\Theta(t,0)} = \left[\frac{\Theta[\mathbf{r}(1)]\Delta t + \Theta[\mathbf{r}(2)]\Delta t + \cdots + \Theta[\mathbf{r}(N)]\Delta t}{N\Delta t}\right], \quad [25]$$

where $\Theta[\mathbf{r}(i)]$ is $\Theta(t, 0)$ for an I–S pair with the internuclear vector $\mathbf{r}(i)$.

To calculate the REDOR dephasing, the three-dimensional powder average must be performed in the same manner as in the multiple-spin case, except now the argument of the cosine is a sum of terms which depends on the trajectory of the moving spin:

$$\frac{S}{S_0} = \frac{1}{8\pi^2} \int_{\psi=0}^{2\pi} \int_{\theta=0}^{\pi} \int_{\phi=0}^{2\pi}$$
$$\times \cos\left[\frac{4\sqrt{2}N_C}{N\nu_R} \sum_{i=1}^{N} \nu_D^i[\hat{n}'(i) \cdot \hat{y}][\hat{n}'(i) \cdot \hat{z}]\right]$$
$$\times d\phi \sin \theta d\theta d\psi. \quad [26]$$

For a rapidly rotating trifluoromethyl group, there are three spins moving relative to the observed ^{13}C nucleus. In this case, the expression in Eq. [22] is combined with the expression in Eq. [26]. Each fluorine contributes one cosine term. The argument of each cosine term is calculated from the position of that fluorine relative to the carbon as the group steps through its circular trajectory. The dephasing is

$$\frac{S}{S_0} = \frac{1}{8\pi^2} \int_{\psi=0}^{2\pi} \int_{\theta=0}^{\pi} \int_{\phi=0}^{2\pi}$$
$$\times \cos\left[\frac{4\sqrt{2}N_C}{N\nu_R} \sum_{i=1}^{N} \nu_D^i[\hat{n}'(i) \cdot \hat{y}][\hat{n}'(i) \cdot \hat{z}]\right]$$
$$\times \cos\left[\frac{4\sqrt{2}N_C}{N\nu_R} \sum_{j=1}^{N} \nu_D^j[\hat{n}'(j) \cdot \hat{y}][\hat{n}'(j) \cdot \hat{z}]\right]$$
$$\times \cos\left[\frac{4\sqrt{2}N_C}{N\nu_R} \sum_{k=1}^{N} \nu_D^k[\hat{n}'(k) \cdot \hat{y}][\hat{n}'(k) \cdot \hat{z}]\right]$$
$$\times d\phi \sin \theta d\theta d\psi. \quad [27]$$

EXPERIMENTS

Spectrometer. Magic-angle spinning ^{13}C and ^{19}F NMR spectra were obtained using a four-channel spectrometer designed for an 89-mm vertical-bore superconducting magnet operating at 4.7 T. Multifrequency tuning was accomplished using a coaxial transmission line connecting tuning components located outside the bore of the magnet to a single, four-turn, 9-mm-i.d. coil (*14*). Chemagnetics 7.5-mm zirconia rotors were spun at speeds up to 6500 Hz with ±2 Hz active control. An ENI LPI-10 1-kW transmitter was used

for the carbon channel, and Kalmus LP-1000 and 166-UP 750 were used on the proton and fluorine channels, respectively. The spectrometer was controlled using a TECMAG Libra pulse programmer.

Samples. Natural-abundance ^{13}C, poly(trifluoroethyl methacrylate) was purchased from Polysciences, Inc. (Warrington, PA). A rotor was packed with 297 mg of the polymer powder without further processing. About 1 mg of a ligand 6-(trifluoromethyl)-7-oxo-8-ribityllumazine was bound to 50 mg of lumazine synthase, the β_{60} subunit of heavy riboflavin synthase from *Bacillus subtilis* (*15*). The sample was lyophilized with both lyoprotectants and cyroprotectants (*16*).

MAS NMR. ^{13}C NMR spectra (Fig. 3) were produced using a 50-kHz matched proton–carbon spin-lock transfer. All ^{13}C chemical shifts were referenced to a secondary external alanine standard with tetramethyl silane as zero. Protons and fluorines were decoupled simultaneously during acquisition of the ^{13}C signal with 100-kHz radiofrequency irradiation on both channels.

^{19}F NMR spectra were acquired using a 90° inspection pulse and a 6-rotor cycle echo. The protons were decoupled with 100-kHz radiofrequency irradiation during echo formation and during the acquisition of the signal. For the enzyme complex, the sample was cooled using −28°C air circulating about the spinning rotor.

REDOR NMR. The ^{13}C-observe (*I* spin), ^{19}F-dephased (*S* spin) REDOR experiment began with a 1-ms cross-polarization transfer from abundant protons. The ^{13}C π pulses were placed at the end of every rotor period to refocus isotropic chemical shifts. The ^{19}F π pulses were applied in the middle of the rotor period every second acquisition. Intensities measured from carbon spectra acquired with (*S*) and without (*S*$_0$) application of the 50-kHz ^{19}F π pulses were used to produce Fig. 5. After cross polarization, the protons were decoupled by 100 kHz of radiofrequency irradiation. During the acquisition of the ^{13}C signal, both protons and fluorenes were decoupled by 100 kHz irradiation.

RESULTS

A magic-angle spinning, CPMAS ^{13}C NMR spectrum of powdered poly(trifluoroethyl methacrylate) is shown in Fig. 3. The spinning sidebands are minor and do not overlap with isotropic peaks. The 125 ppm signal from carbons directly bound to fluorines is well separated from other lines in the spectrum.

The magic-angle spinning ^{19}F NMR spectrum of the 6-trifluoro-7-oxo-8-ribityllumazine β_{60} complex presented in Fig. 4a has a single isotropic peak and a collection of spinning sidebands separated by the 5-kHz rotor frequency. Here the first low-field sideband has 18% and the first high-field sideband 37% of the intensity of the center band. Results
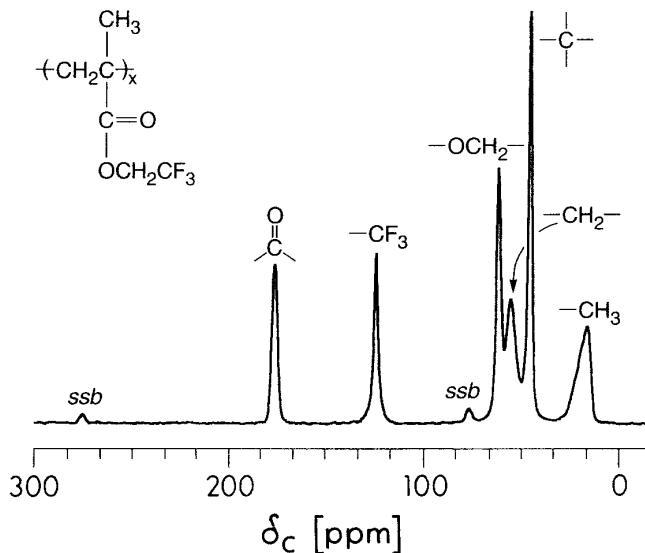

FIG. 3. The 50-MHz cross-polarization, magic-angle spinning ^{13}C NMR spectra of poly(trifluoroethyl methacrylate). The sample was spun at 5 kHz at room temperature. The data were acquired with 19,200 scans using a repetition period of 1 s.

from a similar experiment performed on poly(trifluoroethyl methacrylate) are shown in Fig. 4c. Peak integrations show that the first low-field sideband has 11% and the first high-field sideband 17% of the intensity of the center band.

^{13}C NMR REDOR experiments (with ^{19}F dephasing) were performed on poly(trifluoroethyl methacrylate), and the dephasing (*S*/*S*$_0$) of the 125 ppm –CF$_3$ peak was monitored. The REDOR pulse sequence used to produce the experimental data presented in Fig. 5 had a single ^{13}C-refocusing π pulse. All dephasing π pulses were applied on the ^{19}F channel. REDOR experiments using the Garbow–Gullion sequence (*17*) with a single ^{19}F-dephasing π pulse gave similar results.

DISCUSSION

REDOR of Poly(trifluoroethyl Methacrylate)

To calculate the dephasing for the 125 ppm –CF$_3$ peak, the geometry of the –CF$_3$ group is assumed to be the same as that for trifluoromethane: the C–F internuclear distance is 1.332 Å and the C–F bond forms an angle of 72.0° relative to the C_3 axis of symmetry (*18*). For three spins in motion, the multiple-spin REDOR expression in Eq. [27] was used. This expression has a product of three cosines, one for each fluorine. The arguments of these cosines are sums of terms which depend on the positions of the fluorenes as a function of time. The circular trajectory (of radius 1.267 Å) was modeled with *N* equally spaced steps, and *N* was increased until the calculated REDOR dephasing converged. For the case when the carbon was on the C_3 axis of symmetry,
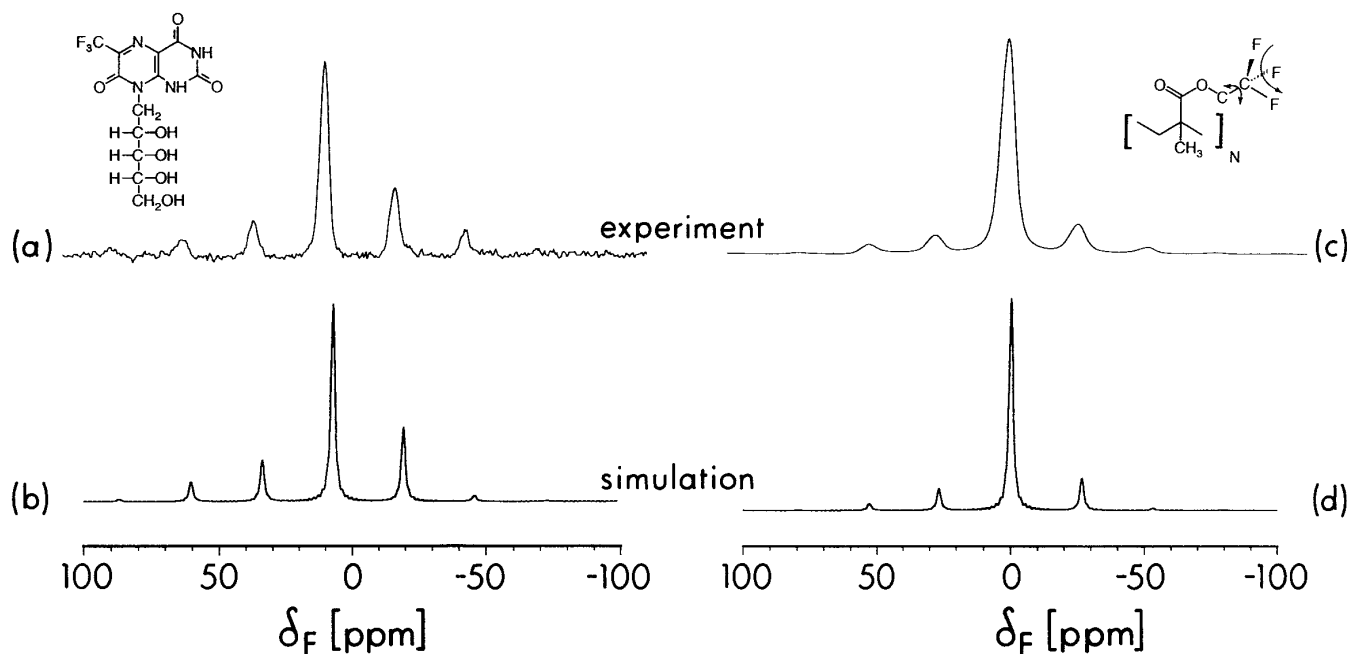
FIG. 4. (a) Experimental, 188-MHz, ^{19}F NMR spectrum of 6-(trifluoromethyl)-7-oxo-8-ribityllumazine bound to lumazine synthase. Magic-angle spinning was at 5 kHz; 1600 transients were acquired with a 2-s repetition period. (b) Simulation of the spectrum in (a) assuming 5-kHz magic-angle spinning and principal values of the chemical-shift tensor of $\sigma_{xx} = 4.8$ kHz, $\sigma_{yy} = 4.8$ kHz, $\sigma_{zz} = -9.6$ kHz. (c) Experimental, 188-MHz, magic-angle spinning ^{19}F NMR spectrum of poly(trifluoroethyl methacrylate). Magic-angle spinning was at 5 kHz; 320 transients were acquired with a 2-s repetition period. (d) Simulation of the spectrum in (c) assuming 5-kHz magic-angle spinning and principal values of the chemical-shift tensor of $\sigma_{xx} = 3.3$ kHz, $\sigma_{yy} = 3.3$ kHz, $\sigma_{zz} = -6.6$ kHz.
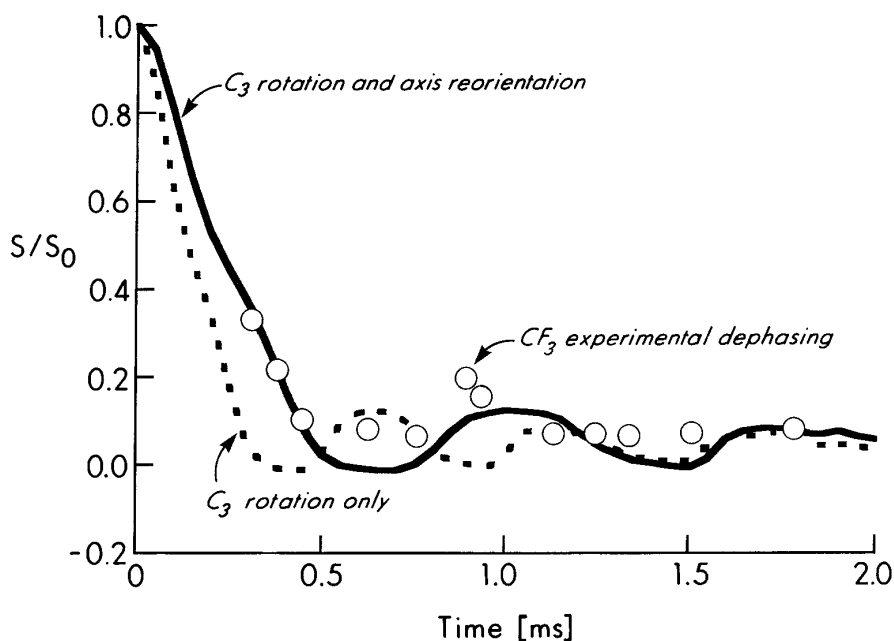

FIG. 5. REDOR dephasing (S/S_0) for the 125 ppm $-CF_3$ carbon peak of poly(trifluoroethyl methacrylate). The open circles represent data acquired for 2, 4, 6, and 8 rotor cycles of dephasing, each with $T_R = 155$, 188, and 222 μs. Accuracy is suggested by the experimental scatter. Reproducibility of S/S_0 for times less than 0.5 μs is within the size of the open-circle symbol. The dashed line is dephasing calculated for ^{13}C REDOR with ^{19}F dephasing assuming fast $-CF_3$ rotation about the C_3 axis and no additional motion. The solid line is this dephasing calculated assuming that the rapidly rotating $-CF_3$ group undergoes 38° isotropic excursions from equilibrium.
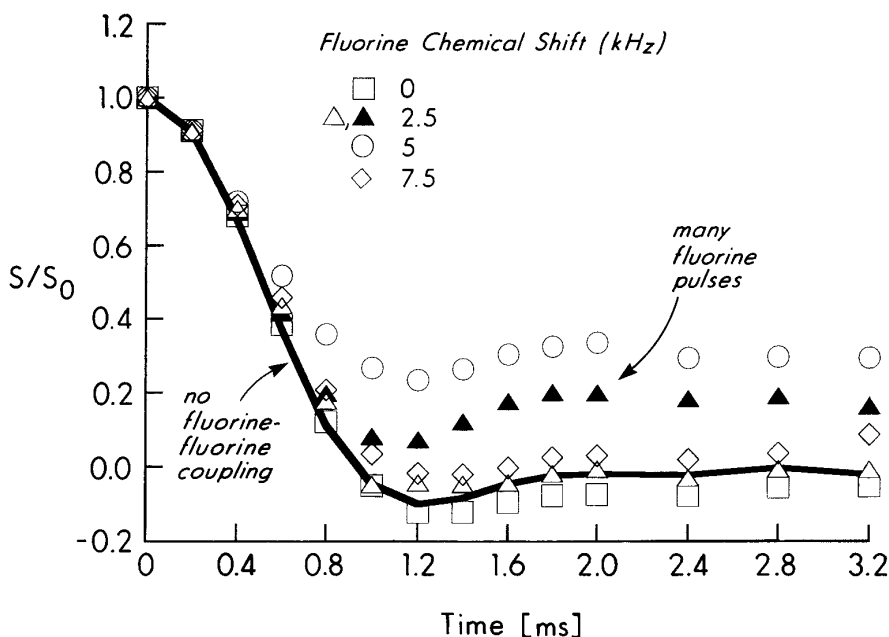
FIG. 6. Simulated ^{13}C REDOR NMR with ^{19}F dephasing for a FCF three-spin system. Two fluorines and a ^{13}C were placed on a 3-Å equilateral triangle. The C–F dipolar coupling was 1052 Hz and the F–F dipolar coupling, 3937 Hz. The simulations assumed no ^{13}C chemical-shift offset, no chemical-shift anisotropy, delta-function pulses, and 5-kHz magic-angle spinning. Different symbols correspond to different ^{19}F isotropic chemical-shift differences (squares, $\Delta\nu_{CS} = 0$ kHz; triangles, $\Delta\nu_{CS} = 2.5$ kHz; circles, $\Delta\nu_{CS} = 5$ kHz; diamonds, $\Delta\nu_{CS} = 7.5$ kHz). For the open symbols, all π pulses were applied on the carbon channel except for a single ^{19}F π pulse in the middle of the evolution period (17). For the filled triangles, one fluorine π pulse was placed in the middle of every rotor period, and one carbon π pulse was placed at the end of every rotor period. The solid line was calculated assuming no F–F homonuclear interaction using Eq. [22].

REDOR dephasings calculated for any $N \geq 3$ were identical (dotted line, Fig. 5). If one assumes that the F–C–F bond angle is exactly tetrahedral (i.e., forms an angle of 70.5° with the C_3 axis), the calculated REDOR dephasing exactly matches that calculated using the formalism suggested by Schaefer *et al.* to describe –CH_3 dipolar patterns for rapidly rotating methyl protons (19).

The smaller ^{19}F chemical-shift sidebands for the polymer –CF_3 group compared to those for the enzyme complex are indicative of molecular motion for the polymer which averages the anisotropic components of the ^{19}F chemical-shift tensor. The –CF_3 group on the polymer is bound to an sp^3 carbon which participates in main-chain reorientational rotations, whereas the –CF_3 group on the enzyme ligand is bound to an sp^2 carbon which is fixed in a rigid, planar configuration.

To quantify the motional averaging due to –CF_3 librations in the polymer, the three principal components of the chemical-shift anisotropy tensor were estimated from the spinning sideband pattern using the Herzfeld and Berger analysis (2). Simulated spectra are shown at the bottom of Fig. 4. The ratio of the sideband intensities to the isotropic peak intensities are within 5% of those for the observed spectra. These results suggest that motion of the –CF_3 group in the polymer is shrinking all three principal components of the shift tensor by the same factor, $\sigma_{ii}^{polymer}/\sigma_{ii}^{complex} = 0.69$ ($ii = xx, yy, zz$).

This motional averaging is consistent with isotropic motion confined inside a cone. In this case, all principal components of any second-rank interaction are scaled by the same factor, $\sigma_{ii}^{cone}/\sigma_{ii}^{static} = (1 - \cos^3\delta)/[2(1 - \cos\delta)] - 1/2$, where δ is the half-angle of the cone (19). Based on the chemical-shift sideband patterns, the –CF_3 group in the polymer apparently undergoes isotropic excursions inside a cone with a 38° half-angle. The C–F dipolar interaction is also scaled by 0.69 because of the librational motion. A calculation of REDOR dephasing with this motionally averaged dipole–dipole interaction strength gives the solid curve in Fig. 5 which is in agreement with the experimental data.

REDOR Dephasing in the Presence of Strong Homonuclear Coupling

Because π pulses do not change the sign of the homonuclear term in Eq. [13], it would appear that this interaction is indeed averaged by magic-angle spinning during a REDOR experiment. However, it is well known that dipolar interactions for homonuclear spin pairs are only partially refocused by magic-angle spinning if the coupled spins have different chemical shifts (20). In fact, the refocusing becomes weakest at ''rotational resonance'' when $n\nu_R$ is equal to the difference in the isotropic chemical shifts $\Delta\nu_{CS}$ (21, 22). We need to know the conditions under which homonuclear couplings

can be neglected when calculating REDOR dephasing for multiple spins.

For an F–C–F triad placed on a 3-Å equilateral triangle, simulations of ^{13}C-observed, ^{19}F-dephased REDOR demonstrate how homonuclear interactions affect REDOR dephasing (Fig. 6). The Garbow–Gullion version of the REDOR experiment with only one ^{19}F dephasing π pulse in the middle of the evolution period (*17, 23*) is least sensitive to the ^{19}F–^{19}F homonuclear interaction. The simulation shows that the REDOR dephasing calculated with a 3.937-kHz homonuclear interaction (open diamonds, triangles, and squares) is close to REDOR dephasing calculated using Eq. [22] (solid line) which corresponds to no homonuclear coupling. Even for strong homonuclear coupling, the approximation used to derive Eq. [22] is valid unless the rotational resonance condition is met (open circles). If, on the other hand, REDOR is performed using a ^{19}F π pulse placed in the middle of every rotor cycle and a ^{13}C π pulse placed at the end of every rotor cycle (solid triangles), neglecting the homonuclear interaction is valid only when the chemical-shift offset between the two fluorine spins is small compared to the rotor speed. The ^{19}F π pulse every rotor period recouples the homonuclear dipole–dipole interaction just as in a SEDRA experiment (*20, 24*). Caution should be exercised in generalizing these results to systems with more than two *S*-spin dephasers in the presence of strong homonuclear couplings. This technique can be used to interpret REDOR dephasing for many *S* spins if the *S*-spin lineshape is inhomogeneously broadened and far from rotational resonance (*10*). If the *S*-spin lineshape is homogeneously broadened, other methods for measuring *I*–*S* dipolar couplings, which employ *S*-spin homonuclear decoupling sequences, are appropriate (*19*).

For a trifluoromethyl group, fast rotation about the C_3 axis ensures that the three fluorine nuclei have identical, motionally averaged chemical shifts. In fact, the time-averaged commutator $\langle [S^i, S^j] \rangle$ is strictly zero as long as the trifluoromethyl group rotates much faster than the F–F dipolar coupling strength. In this fast-exchange limit, the coupling terms of Eq. [13] make no contribution to Eq. [22]. Thus, the strong F–F homonuclear interaction need not be included when calculating ^{13}C REDOR dephasing by ^{19}F in a $-CF_3$ group.

REFERENCES

1. E. O. Stejskal and J. D. Memory, ''High Resolution NMR in the Solid State,'' Oxford Univ. Press, New York, 1994.

2. J. Herzfeld and A. E. Berger, *J. Chem. Phys.* **73,** 6021 (1980).

3. T. Gullion and J. Schaefer, *Adv. Magn. Reson.* **13,** 57 (1989).

4. T. Gullion and J. Schaefer, *J. Magn. Reson.* **81,** 196 (1989).

5. A. W. Hing and J. Schaefer, *Biochemistry* **32,** 7593 (1993).

6. K. T. Mueller, T. P. Jarvie, D. J. Aurentz, and B. W. Roberts, *Chem. Phys. Lett.* **242,** 535 (1995).

7. L. M. McDowell and J. Schaefer, *Current Opinion Struct. Biol.* **6,** 624 (1996).

8. J. M. Griffiths and R. G. Griffin, *Anal. Chim. Acta* **283,** 1081 (1993).

9. L. M. McDowell, M. Lee, R. A. McKay, K. S. Anderson, and J. Schaefer, *Biochemistry* **35,** 3328 (1996).

10. K. L. Wooley, C. A. Klug, K. Tasaki, and J. Schaefer, *J. Am. Chem. Soc.* **119,** 53 (1997).

11. L. M. McDowell, C. A. Klug, D. D. Beusen, and J. Schaefer, *Biochemistry* **35,** 5395 (1996).

12. J. B. Boyce, Thesis, University of Illinois, Urbana–Champaign, 1972.

13. H. Goldstein, ''Classical Mechanics,'' 2nd ed., Appendix B, Addison–Wesley, Reading, MA, 1980.

14. R. A. McKay, U.S. Patent 4,446,413.

15. J. Scheuring, M. Cushman, and A. Bacher, *J. Org. Chem.* **60,** 243 (1995).

16. D. R. Studelska, C. A. Klug, D. D. Beusen, L. M. McDowell, and J. Schaefer, *J. Am. Chem. Soc.* **118,** 5476 (1996).

17. J. R. Garbow and T. Gullion, *J. Magn. Reson.* **95,** 442 (1991).

18. ''Tables of Interatomic Distances,'' Chem. Soc. of London, 1958.

19. J. Schaefer, E. O. Stejskal, R. A. McKay, and W. T. Dixon, *Macromolecules* **17,** 1479 (1984).

20. T. Gullion and S. Vega, *Chem. Phys. Lett.* **194,** 423 (1992).

21. E. R. Andrew, S. Clough, L. F. Farnell, T. A. Gledhill, and I. Roberts, *Phys. Lett.* **21,** 505 (1966).

22. M. H. Levitt, D. P. Raleigh, F. Creuzet, and R. G. Griffin, *J. Chem. Phys.* **92,** 6347 (1990).

23. L. Chopin, R. Rosanske, and T. Gullion, *J. Magn. Reson. A* **122,** 237 (1996).

24. W. Zhu, C. A. Klug, and J. Schaefer, *J. Magn. Reson. A* **108,** 121 (1994).